Enhancement of Near Fields Scattered by Metal-Coated Dielectric Nanocylinders

Pei-Wen Meng, Kiyotoshi Yasumoto, and Yun-Fei Liu
College of Information Science and Technology, Nanjing Forestry University
Nanjing, 210037, China
E-mail: dorismpw@163.com, kyasumoto@kyudai.jp, lyf@njfu.edu.cn

***Abstract*-The scattering of TE polarized plane wave by electrically small metal-coated dielectric cylinders is investigated with a particular emphasis on the enhancement of the near fields. If the wavelength of illumination is properly chosen, two unique near field distributions can be formed along the cylinders. It is shown that the enhanced near fields are localized around two interfaces of the coating metal layer and closely related to the surface plasmon resonances.**

I. INTRODUCTION

With the rapid development of nanoscience and nano-technology, the interaction of light with nanoscaled objects remains as an important topic in recent years because of their promising applications to the optical sensors, imaging, and integrated devices. Enhanced backscattering by multiple nanocylinders under plasmon resonance was theoretically studied in [1]. The visible-light absorption by Si nanowires was discussed in [2]. This explains the optical ignition phenomena. The anomalous light scattering and the peculiarities of the energy flux around a thin wire with surface plasmon resonance were considered in [3]. It presents light scattering by small wires with weak dissipation near plasmon resonant frequencies. The effects of anomalous scattering are too complicated to see in the far field for the majority of metals such as gold, silver and platinum, whereas they can be quite pronounced in the near field region.

In this paper, the scattering of TE polarized plane wave by metal-coated dielectric nanocylinders is investigated with a particular emphasis on the enhancement of the near fields. If the wavelength of illumination is properly chosen, two unique near field distributions can be excited along the cylinders. Numerical results demonstrate that the enhanced near fields are localized around two interfaces of the coating metal layer and closely related to the surface plasmon resonances.

II. FORMULATION OF THE PROBLEM

The cross section of coaxial cylindrical structures to be considered here is shown in Fig. 1. The coaxial cylinder with outer radius r_1 consists of a circular dielectric core with radius r_2 and a metal coating layer of thickness $r_1 - r_2$. The cylinder is infinitely long in the z direction and placed in free space. The material constants of the outer free space, coating metal, and dielectric core are denoted by (ε_0, μ_0), (ε_M, μ_0), and (ε, μ_0), respectively. Fig. 1 shows the configurations of (a) a single coaxial cylinder and (b) two identical coaxial cylinders

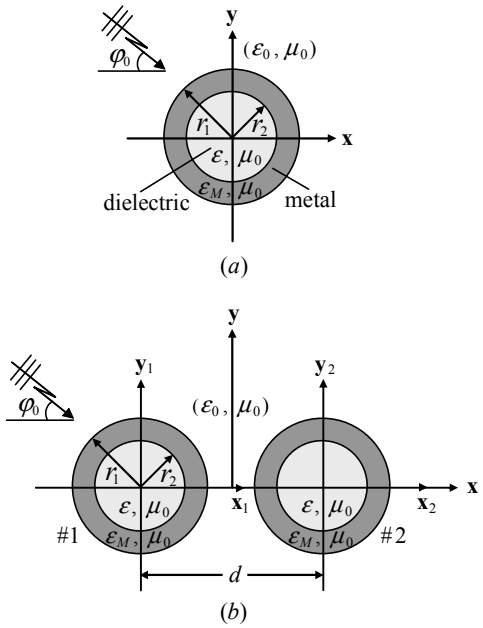

Fig. 1. Cross section of coaxial circular cylinders illuminated by a TE plane wave which is incident normally to the cylinder axis; (a) single cylinder system and (b) two cylinder system.

separated by a distance d along the x axis. The cylindrical structures are illuminated by a plane wave of unit amplitude which propagates normally to the cylinder axis. The angle of incidence of the plane wave is φ_0 with respect to the x axis. The scattering problem is two-dimensional and hence the electric and magnetic fields are decomposed into TE-wave and TM-wave. Since we are interested in the scattering problem related to the plasmon resonances, we focus our investigation on the scattering of TE wave with (H_z, E_x, E_y) component.

Let us consider first the scattering by a single coaxial cylinder shown in Fig. 1(a). The reflection and transmission of the standing and outgoing cylindrical waves at two cylindrical interfaces ($\rho = r_1$ and $\rho = r_2$) are solved separately. This leads to the reflection and transmission matrices for cylindrical harmonic waves at each of the interfaces, which are concatenated to obtain the generalized reflection and transmission matrices over two interfaces. If we denote by the column vectors the set of cylindrical basis function and the set of amplitude coefficients, the solutions to the H_z field in three regions of Fig. 1(a) are obtained, respectively, as follows:

$$H_z = \boldsymbol{\Phi}_0^T \cdot \boldsymbol{p} + \boldsymbol{\Psi}_0^T \cdot \mathbf{T} \cdot \boldsymbol{p} \quad \text{for } \rho > r_1 \tag{1}$$

$$H_z = \boldsymbol{\Phi}_M^T \cdot \mathbf{B} \cdot \boldsymbol{p} + \boldsymbol{\Psi}_M^T \cdot \mathbf{C} \cdot \boldsymbol{p} \quad \text{for } r_2 < \rho < r_1 \tag{2}$$

$$H_z = \boldsymbol{\Phi}^T \cdot \mathbf{D} \cdot \boldsymbol{p} \quad \text{for } 0 < \rho < r_2 \tag{3}$$

with

$$\left.\begin{aligned} &\boldsymbol{\Phi}_0 = [J_m(k_0\rho)\mathrm{e}^{im\varphi}],\ \boldsymbol{\Psi}_0 = [H_m^{(1)}(k_0\rho)\mathrm{e}^{im\varphi}] \\ &\boldsymbol{\Phi}_M = [J_m(k_M\rho)\mathrm{e}^{im\varphi}],\ \boldsymbol{\Psi}_M = [H_m^{(1)}(k_M\rho)\mathrm{e}^{im\varphi}] \\ &\boldsymbol{\Phi} = [J_m(k\rho)\mathrm{e}^{im\varphi}] \end{aligned}\right\} \tag{4}$$

$$\boldsymbol{p} = [p_m],\ p_m = i^m \mathrm{e}^{-im\varphi_0} \tag{5}$$

$$k_0 = \omega\sqrt{\varepsilon_0\mu_0},\ k_M = \omega\sqrt{\varepsilon_M\mu_0},\ k = \omega\sqrt{\varepsilon\mu_0} \tag{6}$$

where J_m $(m = 0, \pm1, \pm2, \cdots)$ is the m-th order Bessel function, $H_m^{(1)}$ is the m-th order Hankel function of the first kind, p_m denotes the amplitude coefficient of the incident plane wave expressed by the cylindrical harmonic expansion. In Eqs.(1)-(3), $\mathbf{T}$, $\mathbf{B}$, $\mathbf{C}$, and $\mathbf{D}$ are diagonal matrices which are defined as follows:

$$\mathbf{T} = [T_m\delta_{mn}],\ T_m = R_{12,m} + \eta_M{}^2 F_{12,m}{}^2 (1 - R_{21,m}R_{23,m})^{-1} R_{23,m} \tag{7}$$

$$\mathbf{B} = [B_m\delta_{mn}],\ B_m = (1 - R_{21,m}R_{23,m})^{-1} F_{21,m} \tag{8}$$

$$\mathbf{C} = [C_m\delta_{mn}],\ C_m = (1 - R_{21,m}R_{23,m})^{-1} R_{23,m} F_{21,m} \tag{9}$$

$$\mathbf{D} = [D_m\delta_{mn}],\ D_m = (1 - R_{21,m}R_{23,m})^{-1} F_{32,m} F_{21,m} \tag{10}$$

where

$$R_{21,m} = -\frac{\eta_M H_m^{(1)}(u_M) H_m^{(1)\prime}(u_0) - H_m^{(1)\prime}(u_M) H_m^{(1)}(u_0)}{\eta_M J_m(u_M) H_m^{(1)\prime}(u_0) - J_m{}'(u_M) H_m^{(1)}(u_0)} \tag{11}$$

$$F_{12,m} = i\frac{2/(\pi\eta_M)}{[\eta_M J_m(u_M) H_m^{(1)\prime}(u_0) - J_m{}'(u_M) H_m^{(1)}(u_0)]} \tag{12}$$

$$R_{12,m} = -\frac{\eta_M J_m(u_M) J_m{}'(u_0) - J_m{}'(u_M) J_m(u_0)}{\eta_M J_m(u_M) H_m^{(1)\prime}(u_0) - J_m{}'(u_M) H_m^{(1)}(u_0)} \tag{13}$$

$$F_{21,m} = \eta_M{}^2 F_{12,m} \tag{14}$$

$$R_{23,m} = -\frac{\xi_M J_m(w_M) J_m{}'(w) - J_m{}'(w_M) J_m(w)}{\xi_M H_m^{(1)}(w_M) J_m{}'(w) - H_m^{(1)\prime}(w_M) J_m(w)} \tag{15}$$

$$F_{32,m} = -i\frac{2/(\pi\xi_M)}{\xi_M H_m^{(1)}(w_M) J_m{}'(w) - H_m^{(1)\prime}(w_M) J_m(w)} \tag{16}$$

$$u_M = k_M r_1,\ u_0 = k_0 r_1,\ w_M = k_M r_2,\ w = k r_2 \tag{17}$$

$$\eta_M = \sqrt{\varepsilon_M/\varepsilon_0},\ \xi_M = \sqrt{\varepsilon_M/\varepsilon}\ . \tag{18}$$

For the two-cylinder system shown in Fig. 1(b), we have to take into account the multiple interactions of the fields scattered from individual cylinders. The interactions can be easily calculated by using the T-matrix $\mathbf{T}$ of the single coaxial cylinder which are defined by Eqs.(1) and (7). Employing two local coordinate systems (ρ_1, φ_1) and (ρ_2, φ_2) whose origins are located at each center of two coaxial cylinders, after straightforward manipulations, the H_z fields in five different regions of the two-cylinder system are derived as follows:

$$H_z = \boldsymbol{\Phi}_0^T \cdot \boldsymbol{p} + \boldsymbol{\Psi}_{0,1}^T \cdot \boldsymbol{a}_1 + \boldsymbol{\Psi}_{0,2}^T \cdot \boldsymbol{a}_2 \quad \text{for } r_1 < \rho_1, \rho_2 \tag{19}$$

$$H_z = \boldsymbol{\Phi}_{M,j}^T \cdot \mathbf{B} \cdot \boldsymbol{q}_j + \boldsymbol{\Psi}_{M,j}^T \cdot \mathbf{C} \cdot \boldsymbol{q}_j \ (j=1,2) \quad \text{for } r_2 < \rho_j < r_1 \tag{20}$$

$$H_z = \boldsymbol{\Phi}_j^T \cdot \mathbf{D} \cdot \boldsymbol{q}_j \ (j=1,2) \quad \text{for } 0 < \rho_j < r_2 \tag{21}$$

with

$$\left.\begin{aligned} &\boldsymbol{\Psi}_{0,j} = [H_m^{(1)}(k_0\rho_j)\mathrm{e}^{im\varphi_j}] \\ &\boldsymbol{\Phi}_{M,j} = [J_m(k_M\rho_j)\mathrm{e}^{im\varphi_j}],\ \boldsymbol{\Psi}_{M,j} = [H_m^{(1)}(k_M\rho_j)\mathrm{e}^{im\varphi_j}] \\ &\boldsymbol{\Phi}_j = [J_m(k\rho_j)\mathrm{e}^{im\varphi_j}] \quad (j=1,2) \end{aligned}\right\} \tag{22}$$

$$\boldsymbol{a}_1 = (\mathbf{I} - \mathbf{T}\boldsymbol{\alpha}_{12}\mathbf{T}\boldsymbol{\alpha}_{21})^{-1}(\mathrm{e}^{-ik_0 d\cos\varphi_0/2}\mathbf{I} + \mathrm{e}^{ik_0 d\cos\varphi_0/2}\mathbf{T}\boldsymbol{\alpha}_{12})\mathbf{T}\cdot\boldsymbol{p} \tag{23}$$

$$\boldsymbol{a}_2 = (\mathbf{I} - \mathbf{T}\boldsymbol{\alpha}_{12}\mathbf{T}\boldsymbol{\alpha}_{21})^{-1}(\mathrm{e}^{ik_0 d\cos\varphi_0/2}\mathbf{I} + \mathrm{e}^{-ik_0 d\cos\varphi_0/2}\mathbf{T}\boldsymbol{\alpha}_{12})\mathbf{T}\cdot\boldsymbol{p} \tag{24}$$

$$\boldsymbol{\alpha}_{12} = [\alpha_{12,mn}],\ \alpha_{12,mn} = H_{m-n}^{(1)}(k_0 d/2) \tag{25}$$

$$\boldsymbol{\alpha}_{21} = [\alpha_{21,mn}],\ \alpha_{21,mn} = (-1)^{m-n} H_{m-n}^{(1)}(k_0 d/2) \tag{26}$$

$$\boldsymbol{q}_1 = \mathrm{e}^{-ik_0 d\cos\varphi_0/2}\,\boldsymbol{p} + \boldsymbol{\alpha}_{12}\cdot\boldsymbol{a}_2 \tag{27}$$

$$\boldsymbol{q}_2 = \mathrm{e}^{ik_0 d\cos\varphi_0/2}\,\boldsymbol{p} + \boldsymbol{\alpha}_{21}\cdot\boldsymbol{a}_1 \tag{28}$$

where $\boldsymbol{\alpha}_{12}$ $(\boldsymbol{\alpha}_{21})$ are the translation matrix which transform $\boldsymbol{\Psi}_{0,2}(\boldsymbol{\Psi}_{0,1})$ to $\boldsymbol{\Phi}_{0,1}(\boldsymbol{\Phi}_{0,2})$ according to the Graf's addition theorem.

III. Numerical Results and Discussions

Equations (1)-(3) and (19)-(21) are used to calculate the near field of H_z for several configurations of metal-coated coaxial cylindrical geometry. It is known that the permittivity of a metal in optical region takes a complex value with a negative real part and a small imaginary part. The value of the real part of the permittivity strongly depends on the wavelength. The proper evaluation of $\varepsilon_M(\lambda)$ for metal is crucial in the analysis. We employ here the Drude-Lorentz model [4] which expresses $\varepsilon_M(\lambda)$ in the following form:

$$\frac{\varepsilon_M(\omega)}{\varepsilon_0} = \varepsilon_\infty - \frac{\omega_{p,D}^2}{\omega(\omega + i\nu_D)} - \Delta_L\frac{\omega_{p,L}^2}{\omega^2 - \omega_{p,L}^2 + i\nu_L\omega} \tag{29}$$

where ε_∞ is the relative permittivity in $\omega \to \infty$, ω_p is the plasma frequency, ν is the collision frequency, Δ_L is the weighting factor for Lorentz mode, and the subscripts D and L are referred to Drude model and Lorentz model, respectively. In the numerical examples, we assumed Ag for the metal and calculated $\varepsilon_M(\lambda)$ using Eq.(29) and the parameters given in TABLE I.

The near field distributions of $|H_z|$ calculated for three different configurations of single cylinder are compared in Fig. 2. The angle of incidence of TE plane wave is $\varphi_0 = 0^\circ$ and the wavelength is $600nm$. The cylinder is (a) a pure dielectric with $r_1 = 40nm$ and $\varepsilon/\varepsilon_0 = 6.5$, (b) a pure metal (Ag) with $r_1 = 40nm$ and $\varepsilon_M/\varepsilon_0 = -13.862 + i0.968$, and (c) a metal

TABLE I
Typical parameters for Ag [4]. All frequencies are given in *THz*.

ε_∞	$\omega_{p,D}/2\pi$	$\omega_{p,L}/2\pi$	$\nu_D/2\pi$	$\nu_L/2\pi$	Δ_L
3.91	13,420	6,870	84	12,340	0.76

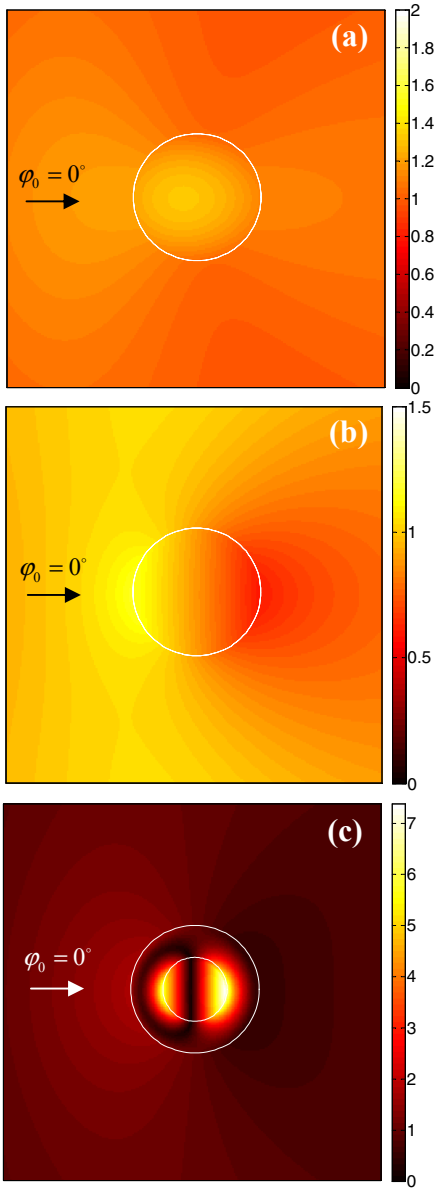

Fig. 2. Comparison of near field patterns of $|H_z|$ for three different configurations of single nanocylinder; (a) a pure dielectric cylinder with $r_1 = 40nm$ and $\varepsilon/\varepsilon_0 = 6.5$, (b) a pure metal (Ag) cylinder with $r_1 = 40nm$ and $\varepsilon_M/\varepsilon_0 = -13.862 + i0.968$, and (c) a metal (Ag)-coated dielectric cylinder with $r_1 = 40nm$, $r_2 = 20nm$, $\varepsilon/\varepsilon_0 = 6.5$, and $\varepsilon_M/\varepsilon_0 = -13.862 + i0.968$. The wavelength is $600nm$.

(Ag)-coated dielectric with $r_1 = 40nm$, $r_2 = 20nm$, $\varepsilon/\varepsilon_0 = 6.5$, and $\varepsilon_M/\varepsilon_0 = -13.862 + i0.968$. The circles depicted by white lines indicate the boundary surfaces of the single and coaxial cylinders. The near field distributions of Figs. 2(a) and 2(b) are conventional, in which we can hardly observe any enhancement of a localized field. In contrast, the near field of the metal-coated coaxial cylinder shows a unique and interesting feature as shown in Fig. 2(c). The incident TE wave penetrates through the metal layer of thickness $r_1 - r_2 = 20nm$ and excites a strong field inside the coaxial cylinder. The excited field is localized in two sides of the cylinder

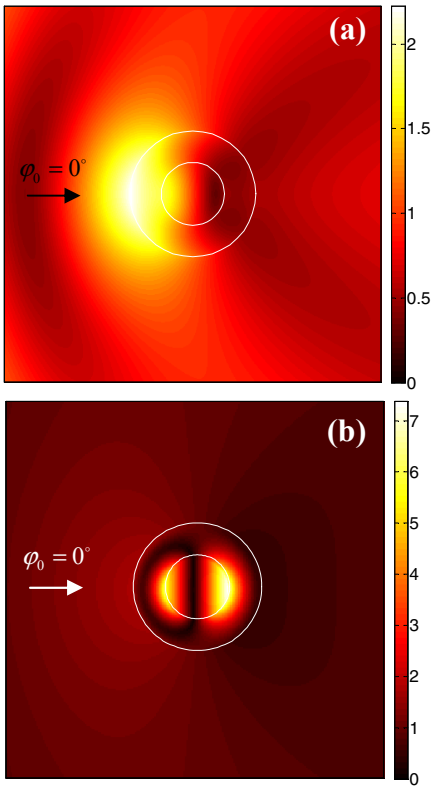

Fig. 3. Near field patterns of $|H_z|$ for the metal (Ag)-coated dielectric nanocylinder with $r_1 = 40nm$, $r_2 = 20nm$, and $\varepsilon/\varepsilon_0 = 6.5$. Two different wavelengths are considered; (a) $\lambda = 314nm$, $\varepsilon_M/\varepsilon_0 = -1.015 + i0.544$ and (b) $\lambda = 600nm$, $\varepsilon_M/\varepsilon_0 = -13.862 + i0.968$.

parallel to the propagation direction of the incident wave and along the interface between the dielectric core and the coating metal (Ag) layer. From the field profile of Fig. 2(c) it follows that the surface plasmon resonance at the inner interface of the metal layer occurs when the wavelength is $\lambda = 600nm$.

In Fig. 3, the near field distributions of $|H_z|$ for the Ag-coated dielectric nanocylinder with $r_1 = 40nm$, $r_2 = 20nm$, and $\varepsilon/\varepsilon_0 = 6.5$ are shown for two different wavelengths. The wavelength and the corresponding $\varepsilon_M(\lambda)$ of Ag are (a) $\lambda = 314nm$, $\varepsilon_M/\varepsilon_0 = -1.015 + i0.544$ and (b) $\lambda = 600nm$, $\varepsilon_M/\varepsilon_0 = -13.862 + i0.968$. For comparison we have reproduced Fig. 2(c) as Fig. 3(b). We can see that the near field pattern in Fig. 3(a) is quite different from that of Fig. 3(b). A strong field is excited only in the illuminated side of the cylinder and along the interface between the metal layer and the outer free space. From the field profile it follows that the surface plasmon supported by the interface between the metal and free space resonates to the incident TE plane wave of $\lambda = 314nm$.

In order to discuss the localized nature of the enhanced field shown in Fig. 2(c) and Fig. 3, we have analyzed the scattered field by a two-cylinder system. Two-identical Ag-coated dielectric nanocylinders with $r_1 = 40nm$, $r_2 = 20nm$, and $\varepsilon/\varepsilon_0 = 6.5$ is placed in parallel to each other. The distance between the centers of two cylinders is $d = 100nm$. Figure 4 shows the near field distributions of $|H_z|$ for two different wave-lengths.

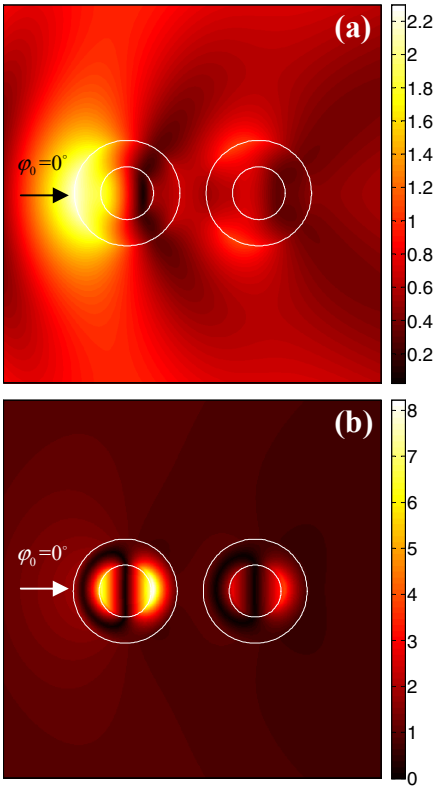

Fig. 4. Near field patterns of $|H_z|$ for two-identical metal (Ag)-coated dielectric nanocylinders with $r_1 = 40nm, r_2 = 20nm$, and $\varepsilon/\varepsilon_0 = 6.5$. The distance between the centers of two cylinders is $100nm$ and the incident angle of plane wave is $\varphi_0 = 0^\circ$. Two different wavelengths are considered; (a) $\lambda = 314nm$, $\varepsilon_M/\varepsilon_0 = -1.015 + i0.544$ and (b) $\lambda = 600nm$, $\varepsilon_M/\varepsilon_0 = -13.862 + i0.968$.

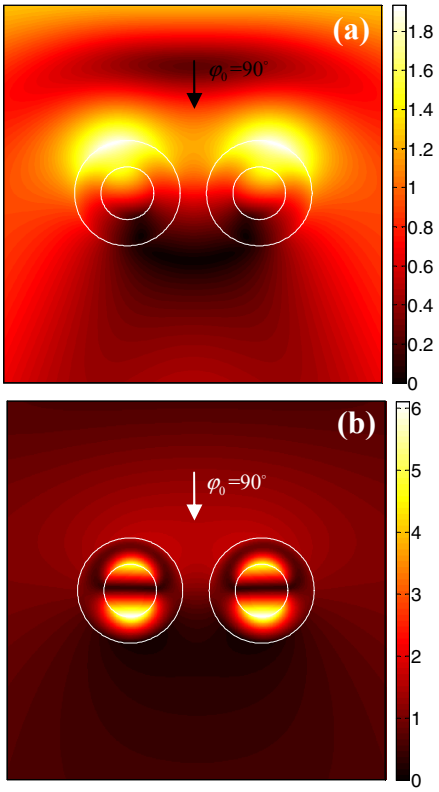

Fig. 5. Near field patterns of $|H_z|$ for two-identical metal (Ag)-coated dielectric nanocylinders. The incident angle of plane wave is $\varphi_0 = 90^\circ$. The others are the same as those in Fig.4.

The incident plane wave with $\varphi_0 = 0^\circ$ propagates in the direction parallel to the array of two cylinders. Since the illumination to the second cylinder is blocked by the first cylinder located in the left-hand side, the major response is governed by the first cylinder. For both wavelengths of $314nm$ and $600nm$, the field patterns are almost same as those shown in Fig. 3, though the maximum of the field intensity is slightly increased in the presence of the second cylinder. Figure 5 shows the near field distributions of $|H_z|$ for the two-cylinder system when the incident plane wave propagates in the direction ($\varphi_0 = 90^\circ$) perpendicular to the array of two cylinders. Since the two cylinders are equally illuminated by the incident plane wave, the localized fields similar to those for a single cylinder shown in Fig. 3 are excited in each of cylinder. There is no noticeable interference between the scattered fields from the individual cylinders.

IV. Conclusion

The scattering of TE plane wave by metal-coated dielectric nanocylinders has been analyzed by using the cylindrical wave expansion and the T-matrix of a circular cylinder. It was shown that two unique near field distributions localized along the nanocylinders are excited when the wavelength of illumination resonates to surface plasmons on either side of the metal layer. For full understanding of light interaction with nanocylinders, it is also required to analyze the scattering cross section, the absorption cross section and their wavelength dependency. This study is under consideration.

Refrences

[1] H. Y. She, L. W. Li, S. J. Chua, W. B. Ewe, O. J. F. Martin, and J. R. Mosig, "Enhanced backscattering by multiple nanocylinders illuminated by TE plane wave," *J. Appl. Phys*., vol. 104, 064310, 2008.

[2] G. Ding, C. T. Chan, Z. Q. Zhang, and P. Sheng, "Resonance-enhanced optical annealing of silicon nanowires," *Phys. Rev.B*, vol. 71, 205302, 2005.

[3] B. S. Luk'yanchuk and V. Ternovsky, "Light scattering by a thin wire with a surface plasmon resonance: Bifurcations of the Poynting vector field," *Phys. Rev. B*, vol. 73, 235432, 2006.

[4] T. Laroche, and C. Girard, "Near-field optical properties of single plasmonic nanowires," *Appl. Phys. Lett*., vol. 89, 233119, 2006.